Dual-action self-healing protective coatings with photothermal responsive corrosion inhibitor nanocontainers

Ma, Lingwei; Wang, Jinke; Zhang, Dawei; Huang, Yao; Huang, Luyao; Wang, Panjun; Qian, Hongchang; Li, Xiaogang; Terryn, Herman A.; Mol, Johannes M.C.

DOI
10.1016/j.cej.2020.127118

Publication date
2021

Document Version
Final published version

Published in
Chemical Engineering Journal

Citation (APA)
Ma, L., Wang, J., Zhang, D., Huang, Y., Huang, L., Wang, P., Qian, H., Li, X., Terryn, H. A., & Mol, J. M. C. (2021). Dual-action self-healing protective coatings with photothermal responsive corrosion inhibitor nanocontainers. *Chemical Engineering Journal*, *404*, Article 127118. https://doi.org/10.1016/j.cej.2020.127118

Chemical Engineering Journal 404 (2021) 127118

Contents lists available at ScienceDirect

Chemical Engineering Journal

journal homepage: www.elsevier.com/locate/cej

Dual-action self-healing protective coatings with photothermal responsive corrosion inhibitor nanocontainers

Lingwei Ma [a,b,c,d,1], Jinke Wang [b,1], Dawei Zhang [a,b,c,*], Yao Huang [b], Luyao Huang [b], Panjun Wang [b], Hongchang Qian [b,c], Xiaogang Li [a,b,c], Herman A. Terryn [e,f], Johannes M.C. Mol [e]

[a] Beijing Advanced Innovation Center for Materials Genome Engineering, Institute for Advanced Materials and Technology, University of Science and Technology Beijing, Beijing 100083, China
[b] National Materials Corrosion and Protection Data Center, University of Science and Technology Beijing, Beijing 100083, China
[c] BRI Southeast Asia Network for Corrosion and Protection (MOE), Shunde Graduate School of University of Science and Technology Beijing, Foshan 528000, China
[d] State Key Laboratory for Marine Corrosion and Protection, Luoyang Ship Material Research Institute (LSMRI), Qingdao 266237, China
[e] Department of Materials Science and Engineering, Delft University of Technology, Delft, Netherlands
[f] Department of Materials and Chemistry, Research Group Electrochemical and Surface Engineering, Vrije Universiteit Brussel, Brussels, Belgium

ARTICLE INFO

Keywords:
Self-healing coating
Photothermal response
Plasmonic titanium nitride
Corrosion inhibitor
Shape memory polymer

ABSTRACT

This work introduces a novel nanocomposite coating with dual-action self-healing corrosion protection activated by the photothermal response of plasmonic titanium nitride nanoparticles (TiN NPs). TiN@mesoporous SiO_2 core–shell nanocontainers were developed as reservoirs for benzotriazole (BTA) corrosion inhibitors and incorporated into the shape memory epoxy coating matrix. Under near-infrared (NIR) light irradiation, the thermogenesis effect of TiN could not only promote the release of corrosion inhibitors from nanocontainers into the crevice, but also trigger the shape memory effect of damaged epoxy to merge the coating scratch. As such, the dual-action self-healing mechanisms combining the formation of an inhibitor-based protective layer and the scratch closure efficiently suppressed the corrosion process at the exposed metal surface. Surface characterization and electrochemical measurement results proved that the nanocomposite coating incorporated with 2 wt% of TiN-BTA@SiO_2 exhibited the optimal corrosion protection as well as an excellent self-healing performance that can be initiated within 30 s of NIR illumination. This photo-controlled self-healing approach is potentially useful in designing next-generation self-healing coatings with ultrafast response time and high healing efficiency.

1. Introduction

Corrosion of metals and alloys is a critical issue in industry fields worldwide, generating huge economic losses as well as safety and environmental hazards.[1–3] To date, organic coatings are the major strategy employed for corrosion protection, providing robust barriers for metals against the permeation of aggressive media.[4–6] However, during the fabrication and service processes, these coatings are susceptible to damages induced by mechanical attacks or environmental degradation. Once the barrier layer is damaged, corrosive agents can easily penetrate through the coating defects and thereby cause the degradation of the underlying metal surfaces.

The concept of self-healing coatings that can spontaneously heal surface damages and recover the protection performance has attracted considerable research interests over the past decade.[7–9] Conventionally, the self-healing function is achieved from two aspects: (1) the repair of the coating matrix by means of reversible chemical bonds [10–13] or physical molecular arrangements;[14,15] (2) the release of healing agents such as reactive monomers,[16,17] thermoplastic additives[18,19] and corrosion inhibitors into the coating defects.[20–22] The self-healing action is often initiated or enhanced in response to external stimuli such as heat,[15,19] light,[4,23] magnetic field[24] and changes in pH[25,26] or corrosion potential.[26,27] More recently, a new kind of stimulation approach based on photothermal conversion has also demonstrated its feasibility in self-healing coatings.[4,9,28] For example, Huang et al.[18] fabricated a polypyrrole (PPy)/

* Corresponding author at: Beijing Advanced Innovation Center for Materials Genome Engineering, Institute for Advanced Materials and Technology, University of Science and Technology Beijing, Beijing 100083, China.
E-mail address: dzhang@ustb.edu.cn (D. Zhang).
[1] Lingwei Ma and Jinke Wang contributed equally to this work.

https://doi.org/10.1016/j.cej.2020.127118
Received 8 July 2020; Received in revised form 7 September 2020; Accepted 20 September 2020
Available online 24 September 2020

polycaprolactone (PCL) hybrid coating, which can quickly heal the coating scratches within 6 min thanks to the photothermal effects of PPy to melt the thermoplastic PCL layers. Zou[29] utilized photothermal-responsive MXene flakes to stimulate the Diels-Alder reaction of epoxy coating, enabling the self-healing performance and the recovery of corrosion protection capability via irradiation of near-infrared (NIR) light at 808 nm. Compared with other stimuli, a photothermal triggered self-healing process offers several advantages for practical applications: [4,18,28] (1) it can be activated remotely and nondestructively to heal the damaged area; (2) it is highly controllable and can be switched on/off instantly; (3) light can be focused on a selected area without distinct interference to the intact coating; (4) compared to the conventional heating and chemical stimulus that require a long time to complete the healing process, the photothermal-triggered healing process is ultrafast (usually within minutes).

A variety of photothermal conversion reagents have been reported, including carbon-based materials[9,10,30] (such as graphene, graphene oxide, carbon nanotube, and carbon black), polydopamine (PDA), [31,32] PPy, [18,23,33] and noble metals. [4,34,35] These materials generally suffer from the drawbacks of high costs and poor dispersion in the polymer matrix. [9,34,36] Recently, titanium nitride nanoparticles (TiN NPs) possessing outstanding plasmonic property have been proved as a promising candidate for photothermal conversion.[37–39] Upon irradiation, the interaction between light and TiN NPs is dramatically enhanced at their resonance wavelength to efficiently collect the light energy. The plasmonic resonance effect significantly increases the yield of conduction electrons, and the coupling between electrons and phonons can elevate the temperature of TiN NPs and surrounding environment over a short time. [35,40] Besides the strong plasmonic effect, TiN NPs possess several other advantages over conventional plasmonic materials (e.g. Au, Ag and Cu), including broad light absorption wavelength in both visible and NIR ranges, superior stability and also low cost.[6,37] These advantages make TiN NPs attractive as light absorbers for a variety of applications such as photothermal therapy,[40,41] water evaporation,[37,42] and anti-icing.[39] Nevertheless, to the best of our knowledge, TiN NPs have not been employed for the development of self-healing coatings.

In the present study, novel core–shell nanocontainers consisting of TiN NPs as cores and mesoporous silica as shells were developed and incorporated into thermoresponsive shape memory polymer (SMP) epoxy coatings to impart ultrafast self-healing performance to their corrosion protection ability. Under NIR light irradiation, the self-healing action by the photothermal effect of TiN is two-fold: (1) the TiN@mesoporous SiO_2 core–shell nanocontainers served as reservoirs for benzotriazole (BTA) corrosion inhibitors, which were efficiently released upon triggering the photothermal effect of TiN cores; (2) the heat generated by the TiN cores could also trigger the shape memory effect of the coating matrix and induce a damage closure effect. The structure and inhibitor release of the BTA-containing TiN@mesoporous SiO_2 NPs (denoted as TiN-BTA@mSiO_2 NPs) were characterized by scanning electron microscopy (SEM), transmission electron microscopy (TEM), Fourier transform infrared (FTIR) and ultraviolet–visible (UV–Vis) spectroscopy. The photothermal effect was activated by an 808 nm NIR irradiation, and the temperature variation of nanoparticles and coatings was recorded by a thermocouple and an infrared camera. The self-healing properties of the coatings were demonstrated by optical microscopy, electrochemical impedance spectroscopy (EIS) and scanning electrochemical microscopy (SECM) measurements.

2. Material and methods

2.1. Materials

TiN NPs, BTA, Bisphenol A diglycidyl ether (DGEBA), neopentyl glycol diglycidyl ether (NGDE), and Jeffamine D230 were purchased from Sigma-Aldrich. Tetraethyl orthosilicate (TEOS) and cetyltrimethylammonium bromide (CTAB) were purchased from Aladdin Chemical Co., Ltd. Other reagents and solvents were supplied by Sinopharm Chemical Reagent. All chemicals and solvents were used as received.

2.2. Preparation of TiN-BTA@mSiO_2 NPs

TiN-BTA@mSiO_2 NPs were synthesized by mixing TiN NPs with BTA inhibitors, CTAB (surfactant molecules) and TEOS (a silica precursor) (see Fig. 1a). To begin with, 0.10 g of TiN NPs were dispersed thoroughly in 120 mL deionized (DI) water at ~ 25 °C using a cell breaker and then transferred to a 250 mL three-necked flask, into which 0.07 g of NaOH was added to adjust the pH value of the system to ~ 12. The mixture was then magnetically stirred at 80 °C in an oil bath. Under stirring, 0.40 g of BTA and 0.25 g of CTAB were added until being dissolved completely. [43] Subsequently, 1.25 mL of TEOS was added dropwise to the mixture. After vigorously stirring the mixture for 2 h, the TiN-BTA@mSiO_2 NPs were obtained and collected by centrifugation at 8000 rpm for 5 min, washed thrice with DI water and dried for 12 h in an oven at 70 °C. For the control experiment, BTA-containing mesoporous SiO_2 NPs without TiN cores were similarly prepared and denoted as BTA@mSiO_2 NPs. Another reference sample was TiN@mSiO_2, from which BTA and CTAB molecules were removed by washing with hydrochloric acid and ethanol followed by drying at 55 °C for 24 h.

2.3. Preparation of self-healing coatings

AA2024-T3 aluminum alloy plates (40 × 30 × 1 mm^3) were used as the coating substrates. Prior to coating preparation, the substrates were abraded by SiC abrasive papers up to 240 grades and then cleaned thoroughly with ethanol. The formulation of the SMP coating consisted of a mixture of DGEBA, NGDE, and Jeffamine D230 at a molar ratio of 1:1:1.[44,45] Different amounts of TiN-BTA@mSiO_2 NPs (1 wt%, 2 wt %, and 3 wt%) were dispersed into DGEBA and NGDE mixture and stirred for 4 h, followed by adding Jeffamine D230 curing agent and stirring continuously.

The prepared resin mixture was first dropped by a pipette to cover the whole surface of the AA2024-T3 substrate, and then spin-coated at 300 rpm for 30 s (Shanghai Chemat Advanced Ceramics Technology, Co., Ltd.) to control the coating thickness and optimize the film uniformity. After that, the coatings were cured at ambient environment for 24 h, and then at 55 °C for 12 h in an oven. The thickness of the dry coatings was ~80 μm. The coatings with 1 wt%, 2 wt%, and 3 wt% TiN-BTA@mSiO_2 NPs were denoted as TBS-1, TBS-2, and TBS-3, respectively. For comparisons, the two reference samples, i.e., the blank epoxy coating without nanofillers, and the coating encapsulated with ~ 1.6 wt % TiN@mSiO_2 NPs (denoted as TS coating), were similarly prepared. The addition of 1.6 wt% TiN@mSiO_2 NPs was to ensure that TS coating and TBS-2 coating had contained the same amount of TiN@mSiO_2 NPs.

2.4. Characterization of the TiN-BTA@mSiO_2 NPs and the coatings

The morphology and elemental mapping of TiN and TiN-BTA@m-SiO_2 NPs were characterized by SEM (Merlin, ZEISS) and TEM (JEM-2100F, JEOL) equipped with energy dispersive spectroscopy (EDS). The chemical structure of the nanoparticles was determined by FTIR (VERTEX 70, Bruker). The plasmonic absorption feature of TiN-BTA@mSiO_2 and BTA@mSiO_2 was obtained by using an UV–Vis spectrometer (Biomate 3s, Thermo Scientific) over a wavelength range of 500–1100 nm. The specific surface area and pore diameter distribution of TiN-BTA@mSiO_2 NPs and TiN@mSiO_2 NPs were determined from N_2 adsorption–desorption isotherms (ASAP2460, Micromeritics instrument Ltd.) using Brunauer-Emmett-Teller (BET) and Barrett-Joyner-Halenda (BJH) methods.[25,43] Numerical simulation of TiN-BTA@mSiO_2 was conducted using the finite element method (FEM) software COMSOL Multiphysics 5.2, under the excitation wavelength of 808 nm.

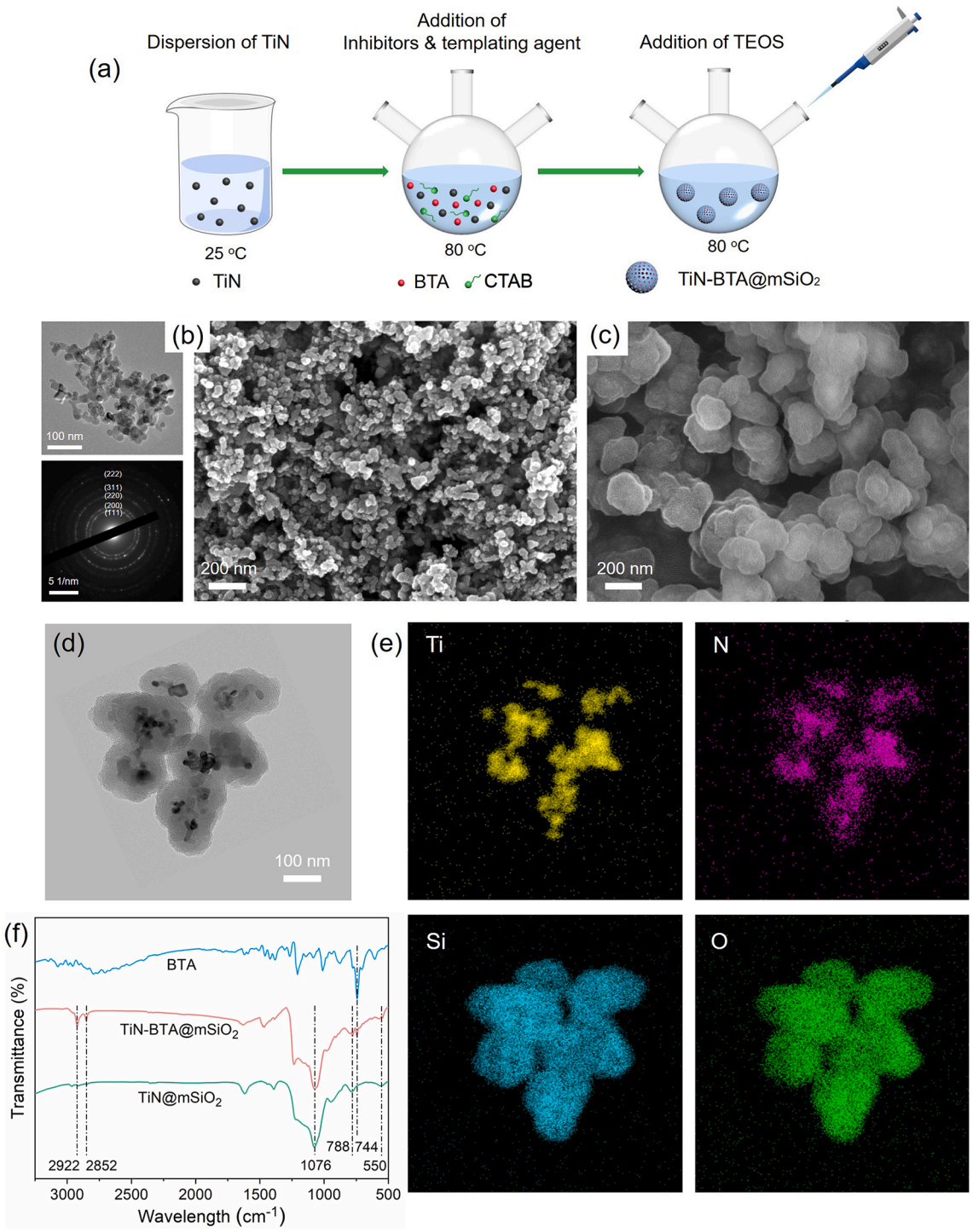

Fig. 1. (a) The schematic diagram of TiN-BTA@$mSiO_2$ NPs preparation; (b) SEM, TEM, and selected area electron diffraction (SAED) results of TiN NPs; (c) SEM image, (d) TEM image, and (e) EDS mapping results of the prepared TiN-BTA@$mSiO_2$ NPs; (f) FTIR spectra of BTA, TiN-BTA@$mSiO_2$ and TiN@$mSiO_2$ NPs.

The thermal properties of the nanocomposite coatings were measured by differential scanning calorimetry (DSC, STA449F3, Netzsch) from 0 °C to 90 °C with a heating rate of 10 °C min^{-1} under nitrogen atmosphere. Raman measurement of inhibitors adsorbed on the AA2024-T3 surface was conducted using a Raman spectroscope (Lab-RAM, Horiba) with a 785 nm laser as the excitation source over the wavelengths of 500–1700 cm^{-1}.

2.5. Inhibitor release behavior

The loading capacity and release profile of BTA in TiN-BTA@$mSiO_2$ NPs were investigated using UV–Vis spectroscopy.[5,43] To obtain the release profile of BTA from TiN-BTA@$mSiO_2$ NPs, 0.04 g of TiN-BTA@$mSiO_2$ NPs were added into a dialysis bag (MW 500) containing 5 mL of 3.5 wt% NaCl solution at different pH values (4.0, 7.0, and 11.0). The dialysis bag was immersed into a beaker containing 100 mL of 3.5 wt% NaCl solution at the corresponding pH and magnetically stirred at 500 rpm. After certain time, 5 mL of the solution outside the dialysis bag

was collected and measured using UV–Vis spectroscopy to determine the amount of released BTA.[46] Standard curves were plotted by recording a series of UV–Vis spectra of the NaCl solution with different BTA concentrations and at different pH values.[47] The solution was poured back into the beaker immediately after UV–Vis analysis and the stirring started again. To analyze the influence of the photothermal effect on the release kinetics of BTA, the TiN-BTA@mSiO_2 solution was irradiated for 5 min by NIR laser (808 nm, 2.5 W/cm^2) [4] at the same time interval as the solution without irradiation, during which UV–Vis absorption measurement was similarly conducted.

2.6. Photothermal conversion performance

To characterize the photothermal conversion effect of the samples, an 808 nm NIR laser (2.5 W/cm^2) was employed as the light source and illuminated on solutions or coating surfaces. The temperature changes were recorded by a thermocouple (Shenzhen Huatu Electric Co., Ltd) and an infrared camera (FLIR ONE PRO, FLIR Systems, Inc.).[10,18,23] The distance between laser source and target sample was kept at 10 cm, and the spot size on the sample surface was about 0.5 cm in diameter.

2.7. Self-healing assessment

To study the self-healing performance of coatings, an artificial scratch was made on each sample surface using a razor blade.[15,19,25] The scratch was ~80 μm in width, ~500 μm in length and penetrated through the coating to reach the metal substrate. The photoinduced healing of the coatings was triggered by the exposure of the scratched region under the NIR laser (808 nm, 2.5 W/cm^2) for 30 s.[4,18] The healing performance was recorded by optical microscope and electrochemical measurements.

2.8. Electrochemical measurements

The corrosion resistance of AA2024-T3 aluminium alloys with different coatings (intact, damaged or healed) was studied in 3.5 wt% NaCl solution by an EIS measurement using an electrochemical workstation (PARSTAT 2273). A conventional three-electrode cell was used, consisting of a saturated calomel electrode (SCE) as the reference electrode, a platinum foil as the counter electrode, and the coated aluminium alloy as the working electrode with an exposed area of 1 cm^2.[14,18] After stabilizing the open circuit potential for at least 30 min, EIS measurement was conducted over the frequency range from 10^5 Hz to 10^{-2} Hz with a sinusoidal voltage perturbation of 20 mV. EIS tests were conducted three times to ensure the repeatability.

Localized corrosion in the scratched regions before and after self-healing was monitored by SECM (CHI 660D) with the substrates immersed in 3.5 wt% NaCl solutions. A four-electrode electrochemical system was employed, with the coated substrate as the working electrode, a platinum coil as the counter electrode, an SCE as the reference electrode, and a platinum microelectrode with the tip diameter of 10 μm as the probe. The distance between microelectrode tip and the coating surface was kept at 25 μm during the measurement. The scanning range was 300 × 300 μm^2 across the scratch area, with a scan rate of 50 μm/s and a tip potential of −0.75 V vs. SCE.

3. Results and discussion

3.1. Preparation and characterization of TiN-BTA@mSiO_2 NPs

Fig. 1a illustrates the fabrication procedure of TiN-BTA@mSiO_2 NPs, the core of which were TiN NPs with a face-centered cubic structure and an average diameter of approximately 35 nm (Fig. 1b). The mesoporous SiO_2 shell with high specific surface area, large pore volumes and favorable stability,[22,25] served as the nanocontainers to encapsulate TiN NPs and to store corrosion inhibitors. The morphology of the as-prepared TiN-BTA@mSiO_2 NPs was characterized by SEM and TEM observations shown in Fig. 1c and 1d, respectively. The nanoparticles displayed a near-spherical morphology with a narrow size distribution ranging from 150 nm to 200 nm. EDS mapping in Fig. 1e provides more detailed information about the distribution of different components in the nanoparticles. The elemental distribution of Si and O outlined the morphology of mesoporous SiO_2. The mapping of Ti and N confirmed that TiN NPs were immobilized in the center of each silica nanocontainers. Moreover, when comparing the elemental mapping of Ti and N, a small portion of N elements were found scatteredly distributed outside the Ti region. These N elements presumably came from the BTA molecules ($C_6H_5N_3$), thereby implying the successful loading of BTA in the TiN-BTA@mSiO_2 NPs.

To identify the chemical composition of the nanoparticles, the FTIR spectra of BTA, TiN-BTA@mSiO_2 and TiN@mSiO_2 (after removing all BTA from the nanoparticles) were obtained (Fig. 1f). The characteristic peaks of both samples were located at 788 and 1076 cm^{-1}, which were assigned to Si-O-Si symmetric stretching and Si-O-Si asymmetric vibration, respectively.[5,43] These bands originated from the formation of mesoporous silica. Besides, there were apparent peaks centered at 550 cm^{-1} for both TiN-BTA@mSiO_2 and TiN@mSiO_2 nanocomposites, representing the Ti-N band of TiN NPs.[41] Compared to TiN@mSiO_2, TiN-BTA@mSiO_2 presented some extra FTIR peaks, corresponding to the C–H in-plane bending vibration of benzene ring of BTA (744 cm^{-1}) and the stretching vibration of C–H bonds of CTAB (2852 and 2922 cm^{-1}).[5,43] Again, these results confirmed the successful encapsulation of TiN and the loading of BTA inside the mesoporous SiO_2 NPs.

During the synthesis of TiN-BTA@mSiO_2, the residual solutions were collected and the BTA concentration was measured using UV–Vis spectra. The amount of the loaded BTA in the nanocontainers was determined by comparing the BTA concentrations in the solutions before and after encapsulation into the nanocontainers. The loading capacity of BTA in TiN-BTA@mSiO_2 NPs was defined as the mass of BTA as a percentage of the total mass of the nanoparticles, which was calculated to be approximately 16.5 wt%. This value was comparable with the mesoporous silica nanocontainers reported in references,[5,22,43] exhibiting high storage ability of corrosion inhibitors in the nanocontainers.

Fig. 2a illustrates the N_2 adsorption–desorption isotherms of TiN-BTA@mSiO_2 and TiN@mSiO_2 NPs. TiN-BTA@mSiO_2 exhibited a very low adsorption capacity of N_2, with a BET surface area of 13.6 m^2/g and no apparent nanopores. After releasing BTA and CTAB from the nanocontainers, a significant increase of N_2 adsorption amount was observed on TiN@mSiO_2 NPs. The N_2 adsorption–desorption isotherm of TiN@mSiO_2 showed a typical type IV isotherm with a clear hysteresis loop,[43,48] implying the presence of a well-defined mesoporous structure. The BET surface area and BJH pore volume were 619.6 m^2/g and 0.65 cm^3/g, respectively. The pore size exhibited a narrow distribution centered at ~ 3.3 nm as shown in Fig. 2b. The highly porous structure of TiN@mSiO_2 ensured the high loading capacity for BTA inhibitors. The strongly decreased specific surface area of TiN-BTA@mSiO_2 indicated the filling of inhibitors into the pores of mesoporous silica.

3.2. Photothermal effect and inhibitor release of TiN-BTA@mSiO_2 NPs

The photothermal effect of TiN can be generated under a plasmonic resonance condition to harvest the light energy and convert the absorbed energy into temperature elevation by the extensive electron–phonon collisions.[39–41] Fig. 3a illustrates the electromagnetic simulation results of TiN-BTA@mSiO_2 NPs under 808 nm laser excitation using FEM under the excitation wavelength of 808 nm. The dimensional parameters of the nanoparticles were acquired from TEM observation in Fig. 1d. The local electric field distribution was intensely enhanced around TiN NPs, indicating that TiN could efficiently absorb light energy and reach the resonance status.[37–39] As shown in Fig. 3b, UV–Vis-NIR absorption spectra were performed to investigate the plasmonic property of

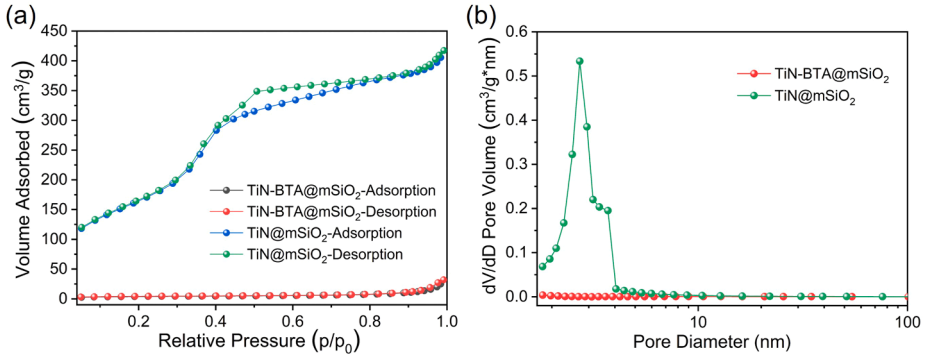

Fig. 2. (a) N_2 adsorption–desorption isotherm and (b) pore diameter distribution of TiN-BTA@$mSiO_2$ and TiN@$mSiO_2$ NPs.

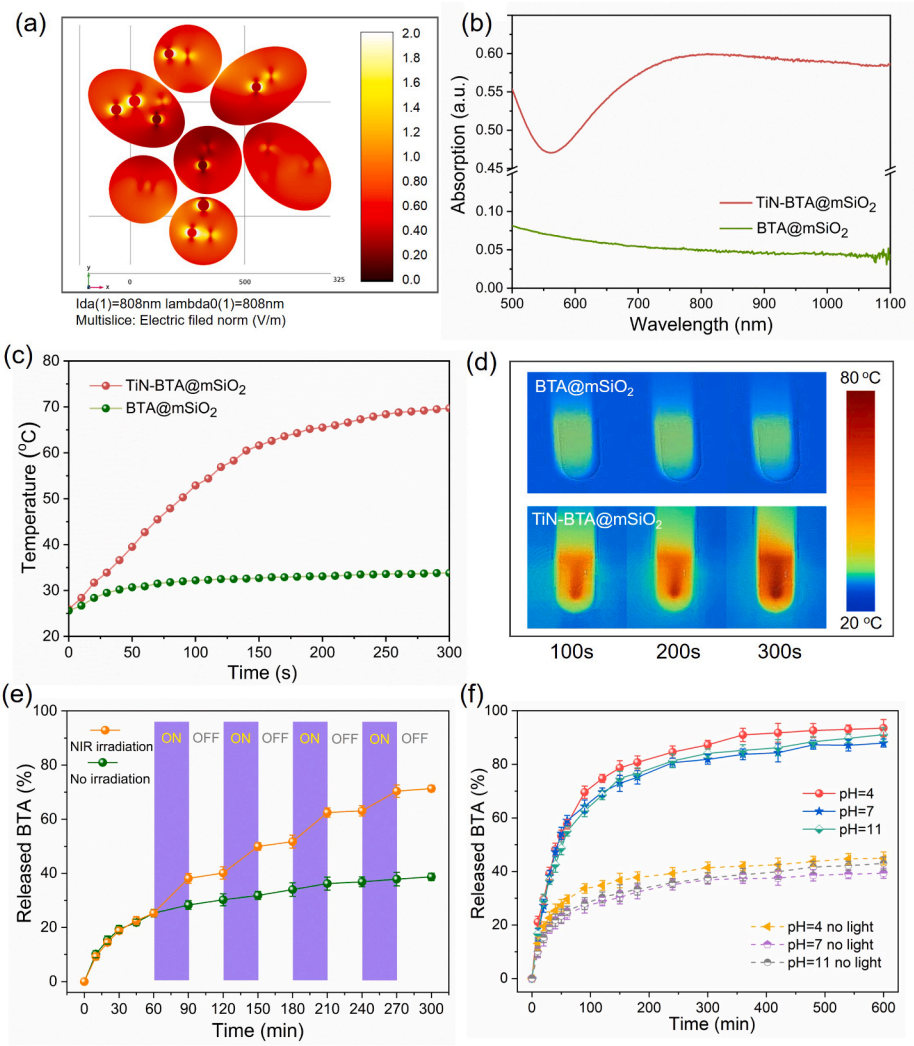

Fig. 3. (a) The electromagnetic simulation results of TiN-BTA@$mSiO_2$ NPs under 808 nm laser excitation; (b) UV–Vis-NIR absorption spectra of TiN-BTA@$mSiO_2$ and BTA@$mSiO_2$ NPs; (c) the real-time temperature variations of solutions containing TiN-BTA@$mSiO_2$ and BTA@$mSiO_2$ NPs, under laser irradiation; (d) the infrared thermal images of solutions containing BTA@$mSiO_2$ and TiN-BTA@$mSiO_2$ NPs, after NIR illumination for distinct time; (e) the release ratio of BTA from TiN-BTA@$mSiO_2$ NPs in neutral NaCl solution with/without NIR irradiation; (f) the time-dependent release profiles of BTA from TiN-BTA@$mSiO_2$ nanocontainers under continuous laser irradiation at different pH conditions.

TiN-BTA@$mSiO_2$ NPs, using BTA@$mSiO_2$ NPs (BTA-containing mesoporous SiO_2 nanoparticles prepared without TiN cores) as a comparison. BTA@$mSiO_2$ NPs possessed a very low light absorption capacity. In comparison, the absorption spectrum of TiN-BTA@$mSiO_2$ NPs displayed a characteristic plasmonic resonance peak located at ~ 800 nm, and sufficient absorption could be observed over a broad Vis-NIR wavelength region.[37,41,42]

The strong light absorption of TiN-BTA@$mSiO_2$ made it very attractive as a thermogenesis material. To visualize the photothermal effect, the temperature variation of the solutions containing TiN-BTA@$mSiO_2$ and BTA@$mSiO_2$ (0.04 g of nanoparticles in 5 mL of DI water) under laser irradiation was monitored (Fig. 3c). Under NIR laser illumination, the temperature of BTA@$mSiO_2$ only increased by ~ 7 °C after 300 s. In contrast, TiN-BTA@$mSiO_2$ exhibited a rapid temperature elevation to ~ 45 °C after 60 s and reached a plateau at ~ 70 °C after 250 s. The local temperature variation was recorded by using an infrared thermal camera. Without TiN (Fig. 3d), there was no detectable temperature rise in the solution containing BTA@$mSiO_2$ NPs within 300 s of

laser irradiation. However, the image of the solution containing TiN-BTA@mSiO$_2$ NPs turned red gradually, implying that the incorporation of TiN NPs brought about a significant photothermal conversion effect.

A rapid release of corrosion inhibitor from the nanocontainers allows for a timely suppression of corrosion activities at the coating defects. However, the release of corrosion inhibitors from the nanoscale porosity of mSiO$_2$ takes place by passive diffusion and is typically slow without external stimulus.[8,25,43] To assess the influence of photothermal effect on the release kinetics of BTA inhibitors from TiN-BTA@mSiO$_2$ NPs, the release profiles of BTA in neutral NaCl solutions with and without NIR irradiation were compared (Fig. 3e). Without light radiation, BTA was released at a relatively low rate. After 300 min, only approximately 40% of the loaded BTA was leached out. In contrast, for the sample being intermittently irradiated by laser, due to the intense photothermal effect from the plasmonic TiN NPs, the BTA release was significantly accelerated. When the irradiation was turned off, the release rate returned back to a slow level, which confirmed that the encapsulation of TiN NPs enabled a photoresponsive regulation of the inhibitor release. The photothermal-controlled release of inhibitors can be effectively regulated according to the specific application and corrosivity of the environment. Fig. 3f shows the release profiles of BTA at different pH conditions under light radiation for 5 min at each UV–Vis measurement interval. The release ratio of BTA was similar at all pH conditions and reached to ~ 90% within 600 min. The photothermally triggered acceleration in BTA release would be beneficial for timely corrosion protection, as the rapid leaching of inhibitors ensures the immediate suppression of corrosion reactions at coating damages.[5,19]

3.3. Photothermal effect and self-healing performance of TBS coatings

Having evaluated the photothermal property of TiN-BTA@mSiO$_2$ NPs, we then incorporated the nanocontainers into the SMP coating. The thermal behavior of the coatings with different amounts of TiN-BTA@mSiO$_2$ NPs was investigated by DSC measurements. As presented in Fig. 4a, the DSC curve of the blank SMP showed an apparent inflection at ~46 °C, which corresponded to the glass transition temperature (T_g) of the epoxy.[14,44] For the coatings containing TiN-BTA@mSiO$_2$ NPs, the DSC curves and T_g remained almost unchanged, suggesting that the presence of a small amount of nanoparticles barely affected the thermal behavior and shape memory effect of the polymer matrix.[14,19] The shape memory effect of SMP coatings depends on its critical T_g. When the surface temperature of the epoxy resin is lower than T_g, the deformation of the coating caused by physical damages is fixed due to the limited mobility of polymer chains. As the temperature increases to above the T_g, the epoxy changes from the glassy state to the rubbery state, which releases the stored strain energy in the deformed area and exerts a contracting force to bring the defect area into spatial proximity. As a result, the shape memory effect leads to the shape recovery of the coating as well as the crack closure.[15,45] Based on the DSC results, we conclude that if the surface temperature of the coating is higher than T_g, the self-healing action can be triggered by the shape memory effect of the coating matrix.[10,18,39]

Thereafter, the thermogenesis effect of TBS coatings (SMP coatings loaded with TiN-BTA@mSiO$_2$ NPs) was assessed upon exposure to NIR laser and monitored via a thermocouple taped on the back side of the

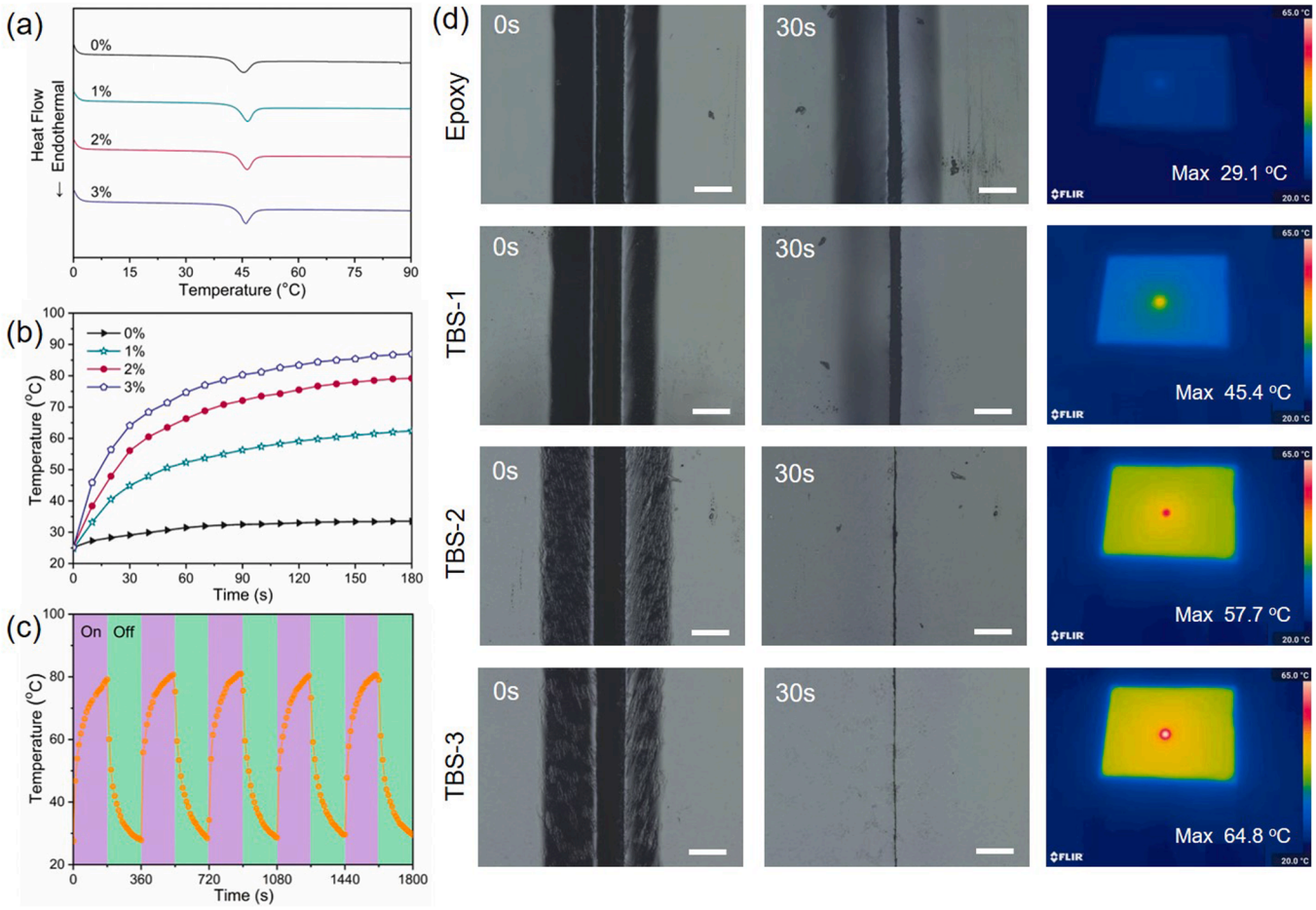

Fig. 4. (a) DSC curves of epoxy coatings with different TiN-BTA@mSiO$_2$ NPs addition amounts of 0%, 1%, 2%, and 3%; (b) the surface temperatures of TBS coatings upon exposure to NIR laser for 180 s; (c) the temperature variations of TBS-2 coating within five on/off irradiation cycles; (d) self-healing and photothermal behaviors of epoxy and TBS coatings under NIR irradiation; scale bar: 100 μm.

AA2024-T3 plate. As shown in Fig. 4b, under laser irradiation, the surface temperatures of TBS coatings increased rapidly within 30 s and reached to a steady state within 180 s owing to the equilibrium between heat generation and dissipation. With the increasing addition of TiN-BTA@mSiO$_2$ NPs, the heating rate increased significantly. The coatings containing 1 wt%, 2 wt%, and 3 wt% nanoparticles reached plateau temperatures of ~ 35 °C, ~55 °C, and ~ 60 °C after 180 s, respectively. In contrast, the blank SMP coating showed negligible temperature elevation (~6 °C) under the same irradiation condition. These observations indicated that the photothermal effect of the coatings could be tailored by the amount of nanofillers. Fig. 4c shows the photothermal stability of TBS-2 coating subjected to five on/off irradiation cycles. Under laser irradiation, the surface temperature of the coating increased substantially; once the laser was switched off, the coating surface rapidly cooled off to room temperature. The cyclic irradiation results manifested that the coating possessed a stable thermogenesis efficiency against repeated NIR irradiation, which is beneficial for multiple coating repairs.

To demonstrate the self-healing performance, an 80 μm wide scratch was made on the TBS coatings using a razor blade and irradiated by the 808 nm laser at a power density of 2.5 W/cm^2 for 30 s. The surface morphologies of the scratch before and after NIR irradiation were recorded by an optical microscope. Besides, infrared thermal images were taken to monitor the thermogenesis behaviors of different coatings. In Fig. 4d, for the blank SMP coating, the width of the scratch showed a limited reduction to ~ 40 μm upon laser irradiation, since its surface temperature (~30 °C) was too low to trigger the shape memory effect. For the TBS-1 coating, the gap was still evident with a width of ~ 30 μm after irradiation. Although the surface temperature of ~ 45 °C was very close to the T$_g$ of TBS coating, the thermal energy was insufficient to efficiently activate the molecular chain motion to heal the crack.[14,34] With an increased TiN-BTA@mSiO$_2$ addition to 2–3 wt%, TiN NPs could absorb and convert more light energy into heat, and rapidly elevated the surface temperatures to be higher than 55 °C. In these cases, the deformed polymer matrix around the coating scratch recovered to its original shape under the shape memory effect, resulting in an evident narrowing of the scratch into a small crevice of only ~10 μm wide. The infrared images in Fig. 4d manifested that during NIR irradiation, the center of the irradiation spots showed the highest temperature, while the temperature of the surrounding area remained relatively low. In other words, the photothermal conversion was localized to the damage region and would minimally affect the property of the intact coating.[24,34]

3.4. Electrochemical measurements

EIS analyses were conducted to investigate the influence of TiN-BTA@mSiO$_2$ NPs on the corrosion protection and self-healing properties of the coatings. The barrier properties of intact coatings were first examined in 3.5 wt% NaCl solution and the results are summarized in Fig. 5a and 5b. After 2 days of immersion, the Nyquist plots of all coatings showed one semicircle, which indicated that corrosion had not occurred on the aluminum alloy substrate.[27,49] The Bode magnitude plots showed a capacitive behavior at 10^5 Hz to 10^1 Hz frequencies and a plateau in the low frequency domain. In the phase angle plots, only one time constant was observed for all coatings, confirming their excellent barrier properties.[26,27,49] Generally, the low-frequency impedance modulus ($|Z|_{0.01\ Hz}$) is an important semi-quantitative parameter to evaluate the corrosion protection performance of coatings.[36,48] Compared to that of the blank coating, the barrier property of the TBS coatings slightly increased with the addition of 1–2 wt% TiN-

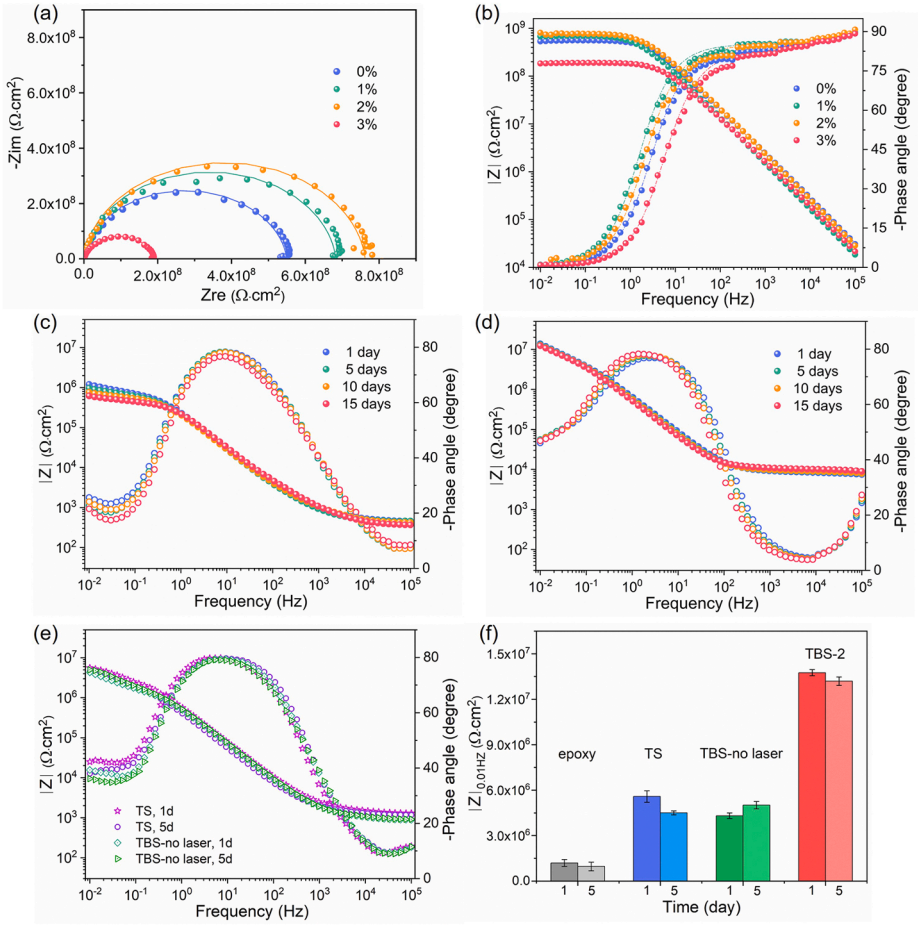

Fig. 5. (a) Nyquist spectra and (b) Bode magnitude and phase angle plots of intact epoxy coatings with different TiN-BTA@mSiO$_2$ NPs addition amounts of 0 wt%, 1 wt%, 2 wt%, and 3 wt%, after immersion in 3.5 wt% NaCl solutions for 2 days; the Bode magnitude and phase angle plots of (c) scratched epoxy coating and (d) the healed TBS-2 coating after immersion in 3.5 wt% NaCl solution within 15 days; (e) the Bode magnitude plots of irradiated TS and TBS-no laser coatings after immersion in 3.5 wt% NaCl solution for 1 day and 5 days; (f) $|Z|_{0.01\ Hz}$ values of distinct samples after immersion in saline solutions for 1 day and 5 days.

BTA@mSiO$_2$, but dropped significantly with the addition of 3 wt%. The inferior barrier property of the TBS-3 coating may be attributed to the agglomeration and non-uniform dispersion of excessive nanoparticles, which introduced more diffusion channels in the coating matrix.[6,17] Based on these results, the TBS-2 coating, exhibiting both excellent shape recovery and high barrier performance, was chosen for the study of the self-healing effect in the following section.

To further evaluate the self-healing effect of the coating, a ~ 80 μm wide scratch was made on the coating surface and then a droplet of water was spread onto the scratched region, followed by NIR laser irradiation for 30 s. The purpose of dropping a small amount of water on the coating surface was to ensure the instantaneous release of BTA inhibitors upon light irradiation. EIS measurements were carried out after immersing the photothermally healed TBS-2 coating in 3.5 wt% NaCl solution for 1, 5, 10, and 15 days, using the damaged blank SMP coating for comparison. In Fig. 5c and 5d, the $|Z|_{0.01\ Hz}$ values of the blank SMP and TBS-2 coatings were 1.2 × 10^6 Ω·cm^2 and 1.4 × 10^7 Ω·cm^2 after 1 day of immersion, respectively. The $|Z|_{0.01\ Hz}$ of blank SMP coating displayed a gradual decrease with a prolonged immersion time as a consequence of the unsuppressed corrosion activity within the wide-open scratch.[6,14,26] In contrast, TBS-2 coating well maintained its $|Z|_{0.01\ Hz}$ values with only a minor descent of ~ 10% over the entire immersion period, which indicated that the corrosion activity on the alloy surface was successfully retarded.[14,20] After 15 days, the $|Z|_{0.01}$

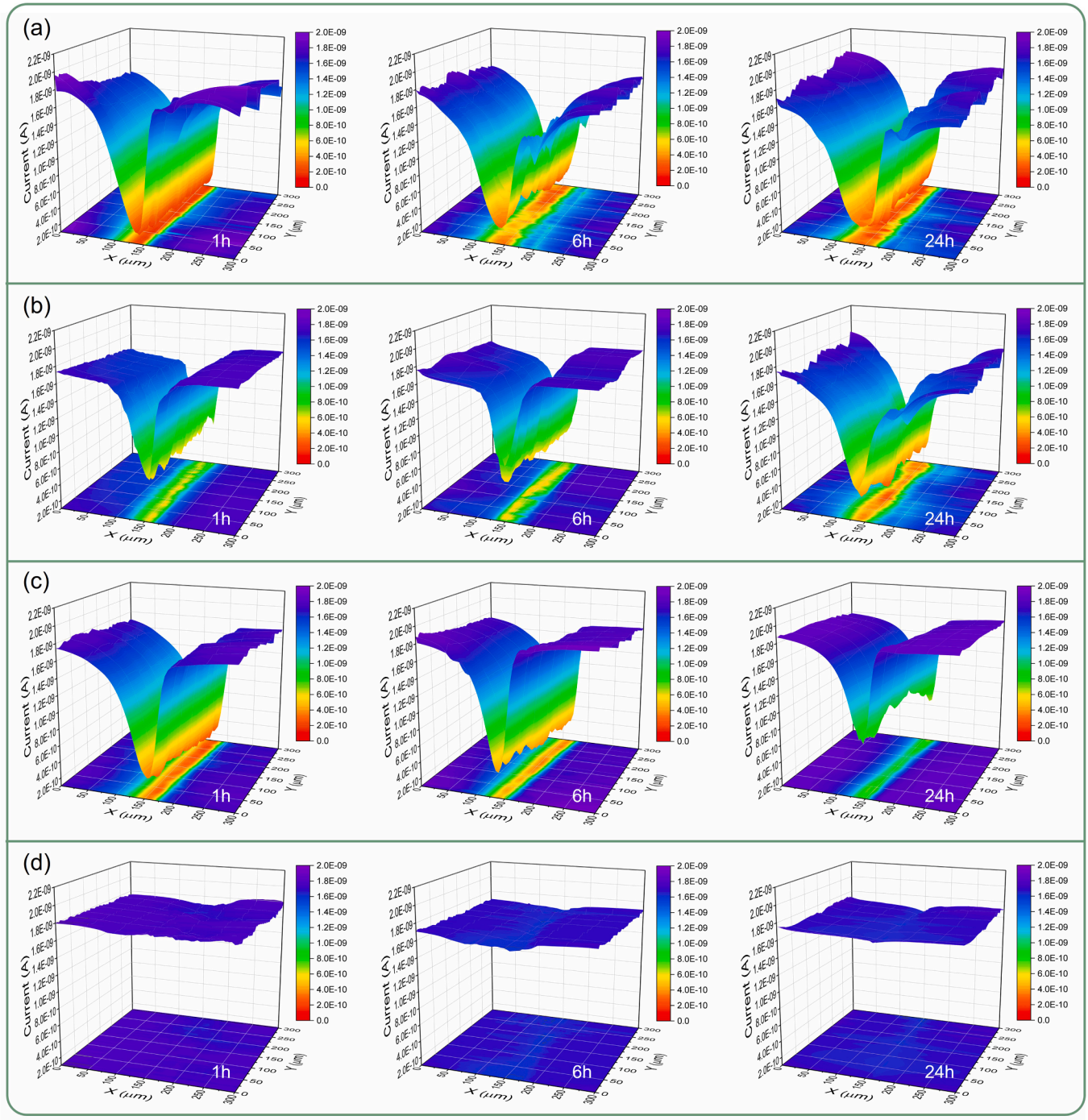

Fig. 6. SECM current mapping of the scratches on (a) blank epoxy coating, (b) TS coating, (c) TBS-no laser coating, and (d) TBS-2 coating, after immersion in 3.5 wt % NaCl solutions for 1, 6, and 24 h.

$_{Hz}$ value of TBS-2 coating (1.2×10^7 Ω·cm^2) was almost 20 times higher than that of the blank epoxy (6.2×10^5 Ω·cm^2), indicating that the photothermally induced self-healing effect strengthened the corrosion protection property. Fig. 5c-5d also present the evolution of phase angles for blank SMP and TBS-2 coatings during the 15-day immersion. Generally, three time constants were shown in the damaged coatings. The time constant in the low frequency range describes the corrosion activity on the underlying metal substrate. The time constant at mid-frequency region is attributed to the formation of oxide layers, which may be composed of native aluminum oxide or the layer formed by the interaction between BTA and the exposed metal surface. The third time constant at high frequency corresponds to the barrier property of the coating.[50] Compared with blank coating, the low-frequency time constant reflecting the corrosion activity disappeared for the TBS-2 coating. Besides, TBS-2 showed much higher phase angle value at 10^5 Hz, implying better corrosion resistance of the nanocomposite coating.[20,25,51]

In order to distinguish the individual effect of scratch closure and inhibitor release on the self-healing performance, two extra samples were prepared and tested, i.e., the coating incorporated with TiN@m-SiO_2 NPs (after removing all BTA from the nanocontainers) and irradiated by NIR light (denoted as TS coating), and the TBS-2 coating without laser irradiation (TBS-no laser coating). As shown in Fig. 5e-5f, the $|Z|_{0.01\ Hz}$ values of both TS and TBS-no laser coatings were higher compared with those of the blank epoxy coating, which suggest that the scratch closure and inhibitor release were both beneficial for the suppression of corrosion activity within the coating scratch. Nevertheless, both of them were much lower than those of the healed TBS-2 coating. The influence of BTA release from individual nanocontainers on the inhibition effect is illustrated in Fig. S1, from which the corrosion inhibition effect of the released BTA molecules was demonstrated. These results clearly manifested that the dual action from the enhanced inhibitor release and the scratch closure and, both triggered by the photothermal conversion, led to the superior self-healing efficiency of the TBS-2 coating.

To further validate the dual-action self-healing performance of the nanocomposite coating, SECM was employed to study the local corrosion activity in the scratch region by monitoring the current intensity of cathodic oxygen reduction on the exposed metal substrate.[14,19] Fig. 6 depicts the mapping of oxygen reduction current around a scratch made on blank coating, TS, TBS-no laser, and TBS-2 coatings, after 1, 6, and 24 h of immersion in 3.5 wt% NaCl solution. As shown in Fig. 6a, the oxygen reduction current within the scratch of blank coating remained at a low level of $\sim 2 \times 10^{-10}$ A during 24 h, indicating the complete consumption of oxygen by the cathodic corrosion reaction on the exposed metal substrate. Without the inhibitor, the TS coating showed slightly increased current values in Fig. 6b, which was attributed to the reduced scratch size after photothermal healing, yet the corrosion activity was still intense. The TBS coating without laser irradiation (Fig. 6c) also exhibited very low current values of around 3×10^{-10} A after 1 and 6 h of immersion. Without the photothermal enhancement, the slow diffusion of BTA from the mesoporous silica nanocontainer could not exert a timely suppression of the severe corrosion activity taking place within the wide-open scratch. After 24 h, the cathodic activity became weaker because of the gradual release and adsorption of BTA.[26,43] On the contrary, once the self-healing effect was photothermally triggered (Fig. 6d), the scratch region presented no remarkable electrochemical activity during the entire 24 h of immersion. The SECM results confirmed, from a micro-electrochemical perspective, that the corrosion activity was effectively suppressed by the dual self-healing actions from inhibitor release and scratch closure.[14,19]

3.5. BTA adsorption and self-healing mechanism

After 24 h of immersion in 3.5 wt% NaCl solution, the healed TBS-2 coating was peeled off from the substrate. Raman measurements were then conducted at different locations on the exposed metal surface to explore the adsorption behavior of BTA. The first detection spot was within the scratch region and the second spot was 2 mm outside the scratch. The third spot was at the intact coating surface which had not been exposed to the corrosive solution. In Fig. 7a, pronounced Raman signals of BTA were collected from the first spot, with characteristic peaks located at 834, 1010, 1146, 1292, 1449 and 1595 cm^{-1}. The peak at 834 cm^{-1} was ascribed to the benzene ring breathing; the peak at 1010 cm^{-1} corresponded to the benzene skeletal and CH bend; the peak at 1146 cm^{-1} was assigned to the NH bend; the peak at 1292 cm^{-1} described the skeletal stretch NH bend and CH bend; and the peak at 1449 cm^{-1} and 1595 cm^{-1} were associated with the benzene ring stretch.[52] These peaks confirmed the presence of a BTA adsorption layer on the alloy surface. At 2 mm from the scratch, the Raman signals of BTA were not as strong as those within the scratch. The metal substrate at this location was still covered by an intact coating without obvious defects. Only a small amount of inhibitors could reach the substrate through diffusion channels within the coating. For the third spot with no direct contact with the saline solution, no Raman signal was detected on the metal substrate. These results clearly demonstrated that the BTA corrosion inhibitors were well stored in the nanocontainers and could be released on demand. Fig. 7b shows the Raman signal at 1010 cm^{-1} mapped over an area of 30×30 μm^2 around the coating scratch. It is shown that the Raman intensity of BTA was very high along the scratch (inside the dotted area), indicating a higher amount of adsorbed inhibitors. The Raman signals were reduced in the surrounding areas covered by the coating. The above observations confirmed that BTA molecules were released from the TiN-BTA@mSiO_2 NPs and had adsorbed on the exposed metal substrate for corrosion protection.

Fig. 8 presents the schematic diagram to explain the dual-action self-healing mechanism of the coating developed in this study. When the coating was damaged, the photothermal effect of TiN NPs could elevate the local temperature under NIR irradiation, generating two responses simultaneously. On one hand, the thermogenesis effect could promote the release of corrosion inhibitors from the nanocontainers to suppress the corrosion activity at the exposed metal surface.[47,53] On the other hand, photothermal response activated the shape memory effect of the polymer matrix, leading to evident scratch closure (from 80 μm to 10 μm) and thus the reduced metal exposure.[14,19,44,54,55] The scratch closure further benefited to minimize the amount of inhibitors required to suppress the corrosion activity. The instant self-healing action upon laser irradiation is a remarkable advantage for healing coating defects where an immediate repair is necessary.

4. Conclusions

In summary, the study reported the development of a dual-action self-healing coating for corrosion protection based on a novel strategy realized by the photothermal-responsive inhibitor-loaded TiN@mSiO_2 nanocontainers and a thermoresponsive SMP epoxy as the coating matrix. Owing to their plasmonic property, TiN NPs could effectively absorb light energy and transform it into heat. Under NIR irradiation, the releasing rate of BTA corrosion inhibitors from TiN-BTA@SiO_2 nanoparticles were dramatically improved; besides, the photothermal effect of TiN rapidly elevated the surface temperature of the coating and triggered the shape memory effect to merge the coating scratch, thus retarding the penetration of corrosive solution. Both EIS and SECM measurements demonstrated that the inhibitor adsorption and scratch closure co-contributed to the effective suppression of corrosion. The coating containing 2 wt% TiN-BTA@SiO_2 NPs exhibited the optimal corrosion resistance as well as a prominent self-healing performance that could be initiated within 30 s of NIR illumination. The ultrafast response time and outstanding self-healing ability, enabled by the photothermally responsive inhibitor nanocontainers as well as the SMP-based coating, may provide new insights for the development of next-generation smart protective coatings.

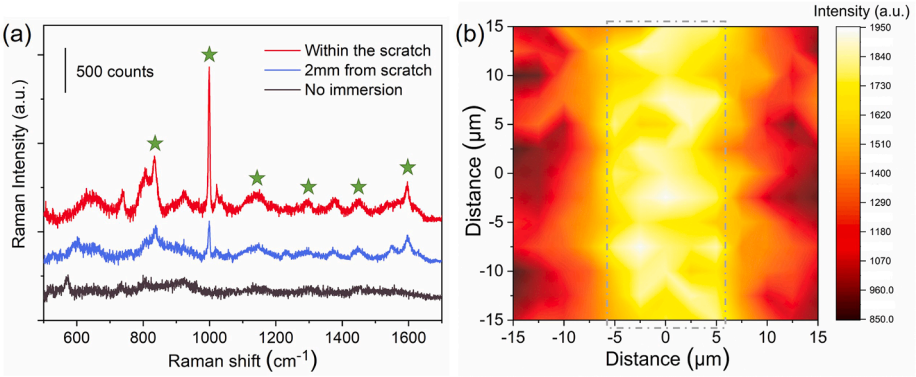

Fig. 7. (a) Raman spectra of BTA molecules on AA2024-T3 substrate surface at different detection positions; (b) Raman intensity mapping of BTA at 1010 cm^{-1} over an area of 30 × 30 μm^2 within the scratch, and X axial direction was perpendicular to the scratch line.

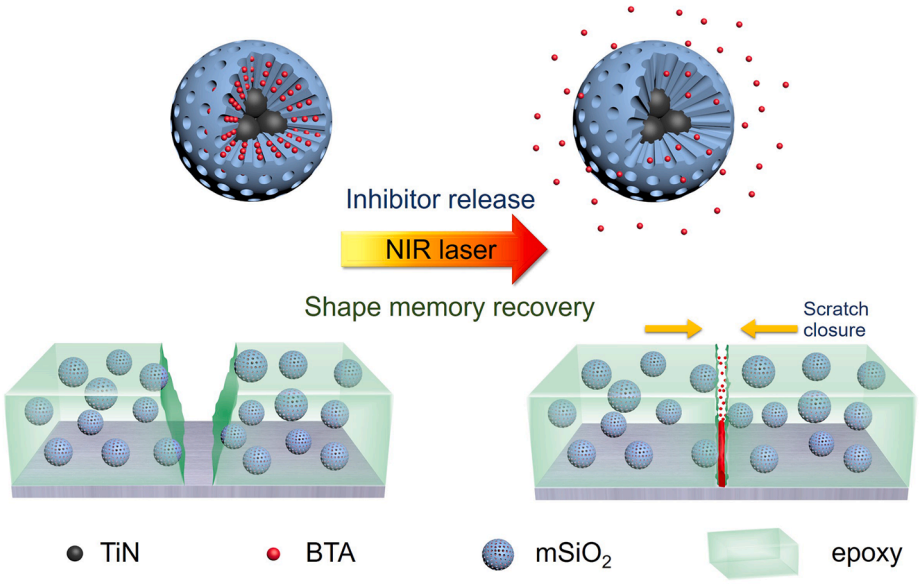

Fig. 8. The schematic diagram of photothermal-triggered self-healing performance of epoxy resin immobilized with TiN-BTA@$mSiO_2$ NPs.

Declaration of Competing Interest

The authors declare that they have no known competing financial interests or personal relationships that could have appeared to influence the work reported in this paper.

Acknowledgements

This work was supported by the National Natural Science Foundation of China (No. 51901015, 51771029), the China Postdoctoral Science Foundation (2018M641189), the Research Fund of State Key Laboratory for Marine Corrosion and Protection, Luoyang Ship Material Research Institute (LSMRI) under the contract No. KFJS1902, and the International Cooperation Fund of Shanghai Science and Technology Commission (No. 17520731800).

Appendix A. Supplementary data

Supplementary data to this article can be found online at https://doi.org/10.1016/j.cej.2020.127118.

References

[1] X. Li, D. Zhang, Z. Liu, Z. Li, C. Du, C. Dong, Materials science: Share corrosion data, Nature 527 (2015) 441–442.
[2] A. Habibiyan, B. Ramezanzadeh, M. Mahdavian, G. Bahlakeh, M. Kasaeian, Rational assembly of mussel-inspired polydopamine (PDA)-Zn (II) complex nanospheres on graphene oxide framework tailored for robust self-healing anti-corrosion coatings application, Chem. Eng. J. 391 (2020), 123630.
[3] B.R. Hou, X.G. Li, X.M. Ma, C.W. Du, D.W. Zhang, M. Zheng, W.C. Xu, D.Z. Lu, F. B. Ma, The cost of corrosion in China, npj Materials Degradation. 1 (2017) 4.
[4] E.V. Skorb, A.G. Skirtach, D.V. Sviridov, D.G. Shchukin, H. Mohwald, Laser-Controllable Coatings for Corrosion Protection, ACS Nano 3 (2009) 1753–1760.
[5] B. Qian, Z. Zheng, M. Michailids, N. Fleck, M. Bilton, Y. Song, G. Li, D. Shchukin, Mussel-inspired self-healing coatings based on polydopamine-coated nanocontainers for corrosion protection, ACS Appl. Mater. Interfaces. 11 (2019) 10283–10291.
[6] Y. Situ, W. Ji, C. Liu, J. Xu, H. Huang, Synergistic effect of homogeneously dispersed PANI-TiN nanocomposites towards long-term anticorrosive performance of epoxy coatings, Prog. Org. Coat. 130 (2019) 158–167.
[7] F. Zhang, P. Ju, M. Pan, D. Zhang, Y. Huang, G. Li, X. Li, Self-healing mechanisms in smart protective coatings: A review, Corros. Sci. 144 (2018) 74–88.
[8] M. Jouyandeh, F. Tikhani, N. Hampp, D.A. Yazdi, P. Zarrintaj, M.R. Ganjali, M. R. Saeb, Highly curable self-healing vitrimer-like cellulose-modified halloysite nanotube/epoxy nanocomposite coatings, Chem. Eng. J. 396 (2020), 125196.
[9] J. Chen, L. Fang, Z. Xu, C. Lu, Self-healing epoxy coatings curing with varied ratios of diamine and monoamine triggered via near-infrared light, Prog. Org. Coat. 101 (2016) 543–552.
[10] J. Bai, Z. Shi, Dynamically cross-linked elastomer hybrids with light-induced rapid and efficient self-healing ability and reprogrammable shape memory behavior, ACS Appl. Mater. Interfaces. 9 (2017) 27213–27222.

[11] H. Ying, Y. Zhang, J. Cheng, Dynamic urea bond for the design of reversible and self-healing polymers, Nat. Commun. 5 (2014) 3218.
[12] Y. González-García, J. Mol, T. Muselle, I. Graeve, G. Assche, G. Scheltjens, B. Mele, H.A. Terryn, A combined mechanical, microscopic and local electrochemical evaluation of self-healing properties of shape-memory polyurethane coatings, Electrochim. Acta. 56 (2011) 9619–9626.
[13] Y. González-García, J. Mol, T. Muselle, I. Graeve, G. Assche, G. Scheltjens, B. Mele, H.A. Terryn, SECM study of defect repair in self-healing polymer coatings on metals, Electrochem. Communi. 13 (2011) 169–173.
[14] H. Qian, D. Xu, C. Du, D. Zhang, X. Li, L. Huang, L. Deng, Y. Tu, J. Mol, H. A. Terryn, Dual-action smart coatings with a self-healing superhydrophobic surface and anti-corrosion properties, J. Mater. Chem. A. 5 (2017) 2355–2364.
[15] L. Wang, L. Deng, D. Zhang, H. Qian, C. Du, X. Li, J. Mol, H. Terryn, Shape memory composite (SMC) self-healing coatings for corrosion protection, Prog. Org. Coat. 97 (2016) 261–268.
[16] D.A. McIlroy, B.J. Blaiszik, M.M. Caruso, S.R. White, J.S. Moore, N.R. Sottos, Microencapsulation of a reactive liquid-phase amine for self-healing epoxy composites, Macromolecules 43 (2010) 1855–1859.
[17] W. Wang, L. Xu, X. Li, Z. Lin, Y. Yang, E. An, Self-healing mechanisms of water triggered smart coating in seawater, J. Mater. Chem. A. 2 (2014) 1914–1921.
[18] L. Huang, J. Li, W. Yuan, X. Liu, Z. Li, Y. Zheng, Y. Liang, S. Zhu, Z. Cui, X. Yang, K. Yeung, S. Wu, Near-infrared light controlled fast self-healing protective coating on magnesium alloy, Corros. Sci. 163 (2020), 108257.
[19] Y. Huang, L. Deng, P. Ju, L. Huang, H. Qian, D. Zhang, X. Li, H.A. Terryn, J. Mol, Triple-action self-healing protective coatings based on shape memory polymers containing dual-function microspheres, ACS Appl. Mater. Interfaces. 10 (2018) 23369–23379.
[20] R. Raj, Y. Morozov, L.M. Calado, M.G. Taryba, R. Kahraman, A. Shakoor, M. F. Montemor, Inhibitor loaded calcium carbonate microparticles for corrosion protection of epoxy-coated carbon steel, Electrochim. Acta. 319 (2019) 801–812.
[21] Y. Feng, Y.F. Cheng, An intelligent coating doped with inhibitor-encapsulated nanocontainers for corrosion protection of pipeline steel, Chem. Eng. J. 315 (2017) 537–551.
[22] D. Borisova, H. Möhwald, D.G. Shchukin, Mesoporous silica nanoparticles for active corrosion protection, ACS Nano 5 (2011) 1939–1946.
[23] Y. Dong, M. Gong, D. Huang, J. Gao, Q. Zhou, Shape memory, self-healing property, and NIR photothermal effect of epoxy resin coating with polydopamine@ polypyrrole nanoparticles, Prog. Org. Coat. 136 (2019), 105232.
[24] L. Huang, N. Yi, Y. Wu, Y. Zhang, Q. Zhang, Y. Huang, Y. Ma, Y. Chen, Multichannel and repeatable self-healing of mechanical enhanced grapheme-thermoplastic polyurethane composites, Adv. Mater. 25 (2013) 2224–2228.
[25] J. Fu, T. Chen, M. Wang, N. Yang, S. Li, Y. Wang, X. Liu, Acid and alkaline dual stimuli-responsive mechanized hollow mesoporous silica nanoparticles as smart nanocontainers for intelligent anticorrosion coatings, ACS Nano 7 (2013) 11397–11408.
[26] T. Wang, J. Du, S. Ye, L. Tan, J. Fu, Triple-stimuli-responsive smart nanocontainers enhanced self-healing anticorrosion coatings for protection of aluminum alloy, ACS Appl. Mater. Interfaces. 11 (2019) 4425–4438.
[27] C. Ding, J. Xu, L. Tong, G. Gong, W. Jiang, J. Fu, Design and fabrication of a novel stimulus-feedback anticorrosion coating featured by rapid self-healing functionality for the protection of magnesium alloy, ACS Appl. Mater. Interfaces. 9 (2017) 21034–21047.
[28] D. Habault, H. Zhang, Y. Zhao, Light-triggered self-healing and shape-memory polymers, Chem. Soc. Rev. 42 (2013) 7244.
[29] Y. Zou, L. Fang, T. Chen, M. Sun, C. Lu, Z. Xu, Near-infrared light and solar light activated self-healing epoxy coating having enhanced properties using MXene flakes as multifunctional fillers, Polymers. 10 (2018) 474.
[30] D. Yi, H. Yoo, S. Mahapatra, Y. Kim, J. Cho, The synergistic effect of the combined thin multi-walled carbon nanotubes and reduced graphene oxides on photothermally actuated shape memory polyurethane composites, J. Colloid Interf. Sci. 432 (2014) 128–134.
[31] S. Xiong, Y. Wang, J. Zhu, J. Yu, Z. Hu, Poly(ε-caprolactone)-grafted polydopamine particles for biocomposites with near-infrared light triggered self-healing ability, Polymer 84 (2016) 328–335.
[32] L. Yang, X. Lu, Z. Wang, H. Xia, Diels-Alder dynamic crosslinked polyurethane/ polydopamine composites with NIR triggered self-healing function, Polym. Chem. 9 (2018) 2166.
[33] G. Qin, J. Qiu, Ordered polypyrrole nanorings with near-infrared spectrum absorption and photothermal conversion performance, Chem. Eng. J. 359 (2019) 652–661.
[34] P. Peng, B. Zhang, Z. Cao, L. Hao, F. Yang, W. Jiao, W. Liu, R. Wang, Photothermally induced scratch healing effects of thermoplastic nanocomposites with gold nanoparticles, Compos. Sci. Technol. 133 (2016) 165–172.
[35] S. Maity, L.N. Downen, J.R. Bochinski, L.I. Clarke, Embedded metal nanoparticles as localized heat sources: An alternative processing approach for complex polymeric materials, Polymer 52 (2011) 1674–1685.
[36] Y. Li, Z. Yang, H. Qiu, Y. Dai, Q. Zheng, J. Li, J. Yang, Self-aligned graphene as anticorrosive barrier in waterborne polyurethane composite coatings, J. Mater. Chem. A. 2 (2014) 14139–14145.
[37] S. Ishii, R.P. Sugavaneshwar, T. Nagao, Titanium nitride nanoparticles as plasmonic solar heat transducers, J. Phys. Chem. C. 120 (2016) 2343–2348.
[38] S. Ishii, K. Uto, E. Niiyama, M. Ebara, Tadaaki Nagao, Hybridizing poly (ε-caprolactone) and plasmonic titanium nitride nanoparticles for broadband photoresponsive shape memory films, ACS Appl. Mater. Interfaces. 8 (2016) 5634–5640.
[39] L. Ma, J. Wang, F. Zhao, D. Wu, Y. Huang, D. Zhang, Z. Zhang, W. Fu, X. Li, Y. Fan, Plasmon-mediated photothermal and superhydrophobic TiN-PTFE film for anti-icing/deicing applications, Compos. Sci. Technol. 181 (2019), 107696.
[40] A. Agrawal, S.H. Cho, O. Zandi, S. Ghosh, R.W. Johns, D.J. Milliron, Localized surface plasmon resonance in semiconductor nanocrystals, Chem. Rev. 118 (2018) 3121–3207.
[41] K.S. Schramke, Y. Qin, J.T. Held, K.A. Mkhoyan, U.R. Kortshagen, Nonthermal plasma synthesis of titanium nitride nanocrystals with plasmon resonances at near-infrared wavelengths relevant to photothermal therapy, ACS Appl. Nano Mater. 1 (2018) 2869–2876.
[42] P. Ren, X. Yang, Synthesis and photo-thermal conversion properties of hierarchical titanium nitride nanotube mesh for solar water evaporation, Sol. RRL. 2 (2018) 1700233.
[43] J. Xu, Y. Cao, L. Fang, J. Hu, A one-step preparation of inhibitor-loaded silica nanocontainers for self-healing coatings, Corros. Sci. 140 (2018) 349–362.
[44] X. Luo, P.T. Mather, Shape memory assisted self-healing coating, ACS Macro Lett. 2 (2013) 152–156.
[45] T. Xie, I.A. Rousseau, Facile tailoring of thermal transition temperatures of epoxy shape memory polymers, Polymer 50 (2009) 1852–1856.
[46] W. Fang, S. Tang, P. Liu, X. Fang, J. Gong, N. Zheng, Pd nanosheet-covered hollow mesoporous silica nanoparticles as a platform for the chemo-photothermal treatment of cancer cells, Small 8 (2012) 3816–3822.
[47] T. Chen, R. Chen, Z. Jin, J. Liu, Engineering hollow mesoporous silica nanocontainers with molecular switches for continuous self-healing anticorrosion coating, J. Mater. Chem. A 3 (2015) 9510–9516.
[48] S. Sanchez-Salcedo, M. Vallet-Regí, S.A. Shahin, C.A. Glackin, J.I. Zink, Mesoporous core-shell silica nanoparticles with anti-fouling properties for ovarian cancer therapy, Chem. Eng. J. 340 (2018) 114–124.
[49] L. Xiong, J. Liu, M. Yu, S. Li, Improving the corrosion protection properties of PVB coating by using salicylaldehyde@ZIF-8/graphene oxide two-dimensional nanocomposites, Corros. Sci. 146 (2019) 70–79.
[50] N.P. Tavandashti, M. Ghorbani, A. Shojaei, J.M.C. Mol, H. Terryn, K. Baert, Y. Gonzalez-Garcia, Inhibitor-loaded conducting polymer capsules for active corrosion protection of coating defects, Corros. Sci. 112 (2016) 138–149.
[51] M. Mahdavian, M.M. Attar, Another approach in analysis of paint coatings with EIS measurement: Phase angle at high frequencies, Corros. Sci. 48 (2006) 4152–4157.
[52] N.R. Honesty, A.A. Gewirth, Shell-isolated nanoparticle enhanced Raman spectroscopy (SHINERS) investigation of benzotriazole film formation on Cu(100), Cu(111), and Cu(poly), J. Raman Spectrosc. 43 (2012) 46–50.
[53] D.G. Shchukin, S.V. Lamaka, K.A. Yasakau, M.L. Zheludkevich, M.G.S. Ferreira, H. Molhwald, Active anticorrosion coatings with halloysite nanocontainers, J. Phys. Chem. C. 112 (2008) 958–964.
[54] X. Zhao, J. Wei, B. Li, S. Li, N. Tian, L. Jing, J. Zhang, A self-healing superamphiphobic coating for efficient corrosion protection of magnesium alloy, J. Colloid. Interf. Sci. 575 (2020) 140–149.
[55] W. Fan, Y. Zhang, W. Li, W. Wang, X. Zhao, L. Song, Multi-level self-healing ability of shape memory polyurethane coating with microcapsules by induction heating, Chem. Eng. J. 368 (2019) 1033–1044.